THE JOURNAL OF PHYSICAL CHEMISTRY Letters

Letter

pubs.acs.org/JPCL

Versatile Titanium Silicide Monolayers with Prominent Ferromagnetic, Catalytic, and Superconducting Properties: Theoretical Prediction

Qisheng Wu, Jun-Jie Zhang, Peipei Hao, Zhongyang Ji, Shuai Dong, Chongyi Ling, Qian Chen, and Jinlan Wang*

Department of Physics, Southeast University, Nanjing 211189, People's Republic of China

Supporting Information

ABSTRACT: On the basis of global structure search and density functional theory calculations, we predict a new class of two-dimensional (2D) materials, titanium silicide (Ti_2Si, $TiSi_2$, and $TiSi_4$) monolayers. They are proved to be energetically, dynamically, and thermally stable and own excellent mechanical properties. Among them, Ti_2Si is a ferromagnetic metal with a magnetic moment of 1.37 μ_B/cell, while $TiSi_2$ is an ideal catalyst for the hydrogen evolution reaction with a nearly zero free energy of hydrogen adsorption. More importantly, electron−phonon coupling calculations suggest that $TiSi_4$ is a robust 2D phonon-mediated superconductor with a transition temperature of 5.8 K, and the transition temperature can be enhanced up to 11.7 K under a suitable external strain. The versatility makes titanium silicide monolayers promising candidates for spintronic materials, hydrogen evolution catalysts, and 2D superconductors.

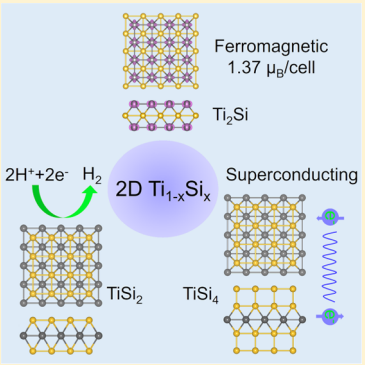

Since the discovery of graphene,[1] the family of two-dimensional (2D) materials[2] has aroused tremendous interest due to their peculiar physical/chemical properties, as well as promising applications in electronics, optoelectronics, energy storage and conversion, hybrid materials, and so on.[3−5] However, these existing 2D materials still cannot meet all practical demands, making it desirable to search new 2D functional materials for accelerating material innovation. Great efforts have been devoted to this field in the past decade, during which theoretical computation won the favor of scientists because it is time- and cost-saving.[6−11] In fact, many newly synthesized 2D materials such as silicene,[12] germanene,[13,14] and borophene[15,16] were first predicted theoretically.[17−22]

Silicon (Si) is the second most abundant element in the Earth's crust (about 28% by mass)[23] and the dominating material in semiconducting electronics. Its 2D form and related layered materials have attracted much attention because they have great advantage of compatibility with the current Si-based electronics industry.[24] To date, except for silicene, which was successfully synthesized via a chemical vapor deposition method,[25] it was predicted computationally that Si can form 2D binary monolayers or few-layer compounds with many nonmetal elements, such as B, C, N, O, P, and S.[26−33] These new 2D binary materials show diverse structural, physical, and chemical properties by controlling atomic ratios. For example, 2D Si_xC_{1-x} monolayers with varying Si concentration ($0 \le x \le 1$) present two structural phases, a homogeneous phase with well-dispersed Si (or C) atoms and an in-plane hybrid phase, which have distinct electronic properties.[31] Silicon phosphide monolayers (Si_xP_y) exist at stoichiometries of $y/x \ge 1$, and their band gaps can be tuned in a wide range by altering the number of layers.[30] 2D SiS monolayers possess suitable direct band gaps and good mobilities for solar cells and nanoelectronics, good flexibility, and air stability.[32,33] Moreover, Si can form binary monolayers with transition metal (TM) elements named TM silicides. Very recently, a Cu_2Si monolayer with planar hexacoordinate copper and silicon was predicted theoretically.[34]

In this Letter, 2D titanium silicide monolayers are globally searched by carrying out particle swarm optimization (PSO) simulations and further studied by density functional theory (DFT) calculations. Titanium (Ti) is selected because it has an equivalent valence electron number of four to Si and may form versatile 2D compounds with Si under different atomic ratios. Among searched structures, Ti_2Si, $TiSi_2$, and $TiSi_4$ are found to be dynamically and thermally stable and own excellent mechanical properties. Moreover, they are all metallic, and Ti_2Si is ferromagnetic with a magnetic moment of 1.37 μ_B/cell while $TiSi_2$ is an ideal hydrogen evolution catalyst with a nearly zero hydrogen adsorption free energy. Most interestingly, $TiSi_4$ is predicted to be a 2D phonon-mediated superconductor with a transition temperature (T_c) of 5.8 K, and the T_c can be further increased up to 11.7 K under suitable external strain. If synthesized, titanium silicide monolayers will greatly enrich the family of 2D materials.

Figure 1a−c displays the optimized structures of Ti_2Si, $TiSi_2$, and $TiSi_4$. In Ti_2Si, each unit cell contains one Si atom and two

Received: August 3, 2016
Accepted: September 7, 2016

DOI: 10.1021/acs.jpclett.6b01731
J. Phys. Chem. Lett. 2016, 7, 3723−3729

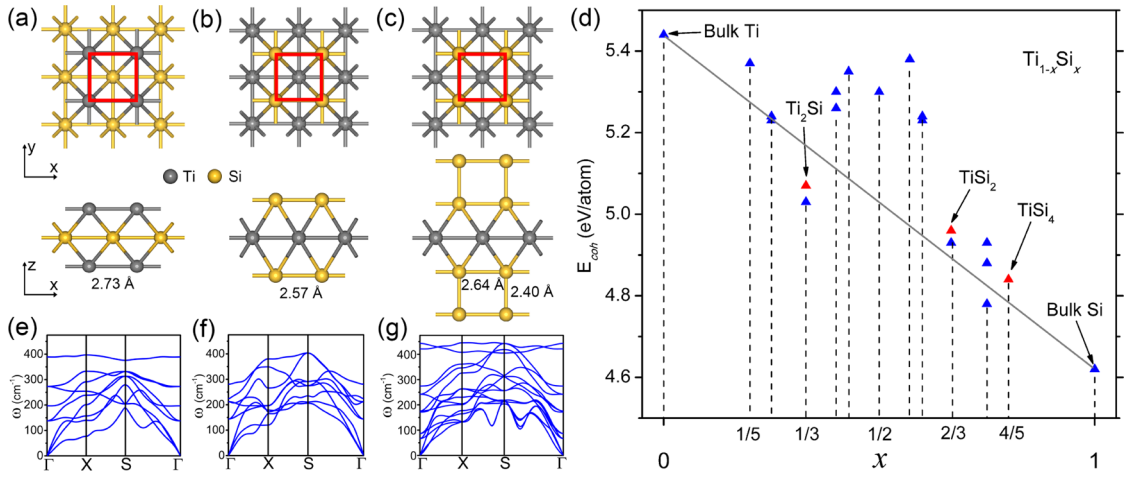

Figure 1. (a–c) Top views (up panels) and side views (bottom panels) for 2 × 2 supercells of Ti_2Si (a), $TiSi_2$ (b), and $TiSi_4$ (c). Red squares in (a–c) stand for primitive cells. (d) Cohesive energies E_{coh} versus composition x for titanium silicide monolayers as listed in Figure S1. Data points for bulk Ti and bulk Si are connected with a solid gray line. Comparisons with that of bulk Ti and bulk Si are drawn. Data points for Ti_2Si, $TiSi_2$ and $TiSi_4$ are labeled in red. (e–g) Phonon dispersions for Ti_2Si (e), $TiSi_2$ (f), and $TiSi_4$ (g).

Ti atoms. This monolayer is in tetragonal symmetry, and its lattice constants are $a = b = 2.73$ Å, belonging to space group $P4/mmm$. $TiSi_2$ and $TiSi_4$ have the same symmetry as that of Ti_2Si, with the Ti atoms located in the middle. In particular, for $TiSi_4$, the Ti layer is sandwiched by two completely parallel silicon layers at each side. Detailed structural information on Ti_2Si, $TiSi_2$, and $TiSi_4$ is given in Table S1. Bader charge[35] analyses show that there is apparent charge transfer from Ti atoms to Si atoms (see Table S1), indicating the ionic nature of Ti–Si bonds. Interactions among in-plane Si atoms are clearly weakened due to the elongation of the Si–Si bond length (equal to corresponding lattice constants) in comparison to those in a Si single crystal (2.35 Å). There is one exception, that is, the short bonds between Si atoms in the topmost layer and those in the second layer (2.40 Å) in $TiSi_4$ make their bonding completely covalent.

To evaluate the stability of these titanium silicide monolayers, we computed the cohesive energy, defined as $E_{coh} = (1 - x)E_{Ti} + xE_{Si} - E_{Ti_{1-x}Si_x}$ $(0 \le x \le 1)$, where E_{Ti}, E_{Si}, and $E_{Ti_{1-x}Si_x}$ are the total energies of a single Ti atom, a single Si atom, and corresponding titanium silicide monolayers, respectively. The cohesive energies of Ti_2Si, $TiSi_2$, and $TiSi_4$ are 5.07, 4.96, and 4.84 eV/atom, respectively. To give a much more realistic picture, we made a simple cohesive energy diagram,[36] E_{coh} versus composition x (of $Ti_{1-x}Si_x$), as shown in Figure 1d. The data points for Ti_2Si, $TiSi_2$, and $TiSi_4$ are located very close to or above the line connecting that for bulk Ti and bulk Si, indicating their high stability and feasibility of synthesis in experiment. Their dynamical stability is further verified by phonon dispersion calculations, which show no imaginary frequency in the Brillouin zone, as displayed in Figure 1e–g. This means that Ti_2Si, $TiSi_2$, and $TiSi_4$ are dynamically stable and local energy minima. The highest frequencies can reach more than 400 cm^{-1} (exhaustive analyses on vibrational modes are given in Figure S2), suggesting the strong interaction between Ti and Si atoms. Moreover, ab initio molecular dynamics (AIMD) simulations demonstrate that these titanium silicide monolayers are also highly stable at ambient conditions. As shown in Figure S3, Ti_2Si, $TiSi_2$, and $TiSi_4$ can maintain their monolayer structures after annealing at 300 and 600 K for 5 ps. Although Ti_2Si and $TiSi_2$ begin to collapse at a temperature of 900 K, $TiSi_4$ still holds good shape, showing the best stability among these three structures.

The existence of strong covalent bonding in $TiSi_4$ directly brings about excellent mechanical property. The computed in-plane stiffness (see the methods in the Supporting Information) of $TiSi_4$ is as high as 292 N/m, which is comparable to that of graphene (342 N/m).[37] Even for Ti_2Si and $TiSi_2$ without strong covalent bonding, the in-plane stiffness reaches about ~120 N/m, almost the same as that of $MoSe_2$ (125 N/m)[38] and twice greater than that of silicene (61 N/m).[37] Further calculations of stress–strain relations for different cells under equi-biaxial strain (see Figure S4) show that the strain at maximum stress is around 0.11–0.14 for predicted titanium silicide monolayers, again demonstrating their prominent mechanical properties.

Besides their excellent mechanical properties, can these titanium silicide monolayers own other fantastic electronic or magnetic properties? As clearly shown in Figure 2, number of bands across the Fermi Level, indicating that these monolayers are all metallic. The density of states (DOS) further reveals that the bands around the Fermi level are mainly from Ti 3d orbitals for Ti_2Si. With the increase in the proportion of Si atoms, apparent hybridization appears between Ti 3d orbitals and Si 3p orbitals for $TiSi_2$ and $TiSi_4$. Moreover, Ti_2Si is found to be ferromagnetic with a magnetic moment as high as 1.37 μ_B/cell, while $TiSi_2$ and $TiSi_4$ are both nonmagnetic. The spin density analysis shows that the high magnetic moment in Ti_2Si is mainly contributed by Ti 3d orbitals (see the inset in Figure 2a). Note that the ferromagnetism of Ti_2Si is rather robust. DFT+U calculations indicate that the energy difference between the ferromagnetic state and antiferromagnetic state (or nonmagnetic state) is enlarged with the increase of the U value, and the magnetic moment is enhanced as well (up to ~2.0 μ_B/cell).

Very recently, it was found that turning semiconducting 2H-MoS_2 into metallic 1T-MoS_2 can greatly enhance the hydrogen evolution reaction (HER), which is derived from the large DOS at the Fermi level and a number of active sites in the 1T phase.[39] As the titanium silicide monolayers are all intrinsically metallic and have similar sandwich structures as MoS_2, they may hold excellent HER catalytic activity as well. Theoretically,

DOI: 10.1021/acs.jpclett.6b01731
J. Phys. Chem. Lett. 2016, 7, 3723–3729

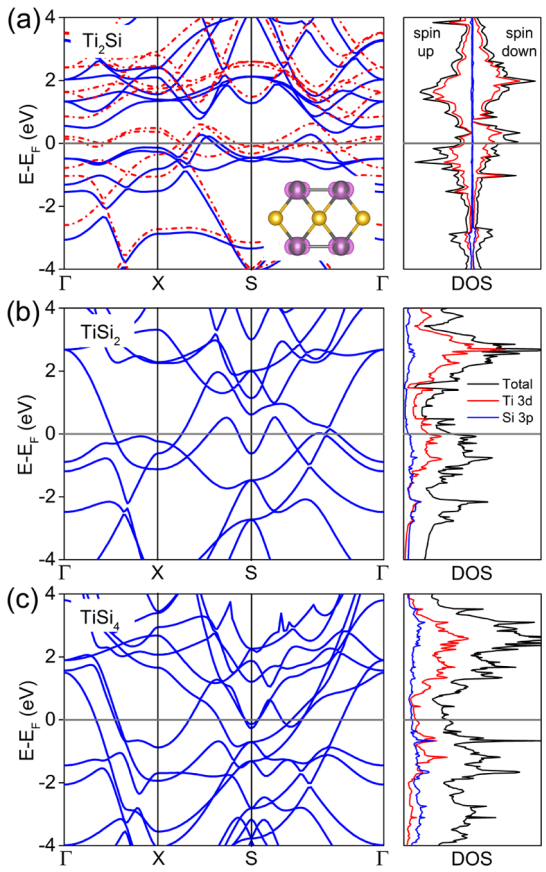

Figure 2. (a–c) Band structures (left panels) and electronic DOS (right panels) of Ti_2Si (a), $TiSi_2$ (b), and $TiSi_4$ (c). The Fermi level is set to be zero and labeled with a solid gray line. For Ti_2Si, the blue solid and red dashed lines in the band structure stand for spin-up and spin-down bands, respectively. The spin density distribution (in violet) for Ti_2Si is drawn inside. Contributions from Ti 3d and Si 3p orbitals are marked in the electronic DOS.

the Gibbs free energy of hydrogen adsorption (ΔG_H) in the reaction is widely used to assess the HER catalytic activity of materials. The ΔG_H can be calculated according to the formula[40] $\Delta G_H = \Delta E_H + \Delta E_{ZPE} - T\Delta S_H$, in which ΔE_H is the binding energy of a hydrogen atom, $\Delta E_H = E_{(System+H)} - E_{System} - (1/2)E_{H_2}$, where $\Delta E_{(System+H)}$ and ΔE_{System} are the energies of the catalyst with and without H adsorption, respectively. ΔE_{ZPE} and ΔS_H are the zero-point energy difference and entropy difference between the adsorbed and gas phase, respectively. The term $\Delta E_{ZPE} - T\Delta S_H$ is calculated to be 0.21 eV for Ti_2Si and 0.26 eV for $TiSi_2$ and $TiSi_4$ (T = 298 K). For Ti_2Si, the H binding is very strong (ΔE_H = −1.05 eV) because the H atom tends to locate at the hollow site and bind with four Ti atoms (see Figure S5). The strong binding makes ΔG_H as small as −0.84 eV and hampers its application for the HER. For $TiSi_2$, the ΔE_H increases to −0.24 eV, and the corresponding ΔG_H is only 0.02 eV. This value is even closer to zero than that for the Pt(111) surface (−0.09 eV), suggesting that $TiSi_2$ is probably an excellent catalyst for HER activity. Regarding $TiSi_4$, the Si atoms at the topmost layer form covalent bonds with neighboring Si atoms. As a result, there is no dangling bond left for $TiSi_4$ to bind with the H atom, leading to a positive ΔE of 0.50 eV and a large ΔG_H of 0.76 eV; thus, it is not a good catalyst for the HER.

It is known that an increase in the coverage of H adsorption may damage the catalytic activity, as has been identified in many TM dichalcogenide monolayers such as MoS_2, VS_2, and $NbSe_2$.[41,42] Thus, it is vital to design new catalysts that can maintain good activity under high H coverage, as perfectly presented in the Pt catalyst.[40] The effect of H coverage, defined as the ratio of the number of adsorbing H atoms with respect to the number of exposed Si atoms, on the HER efficiency is explored by using a 4 × 4 supercell of $TiSi_2$. The lowest energy profiles of H atom adsorption are depicted in Figure S6. Clearly, $TiSi_2$ remains in good shape upon adsorption of H atoms, implying that it also has good chemical stability. The calculated $|\Delta G_H|$ is no larger than 0.1 eV for most coverages, as shown in Figure 3b, suggesting that $TiSi_2$ has comparable HER performance with the Pt surface even under high H coverage.[40]

In fact, a complete HER is a multistep reaction that includes electrochemical hydrogen adsorption (Volmer reaction) and electrochemical desorption (Heyrovsky reaction) or chemical desorption (Tafel reaction). The above discussion belongs to the Volmer reaction. Generally speaking, the catalyst that has high activity for the Volmer reaction will have the same catalytic activity for the Heyrovsky reaction. Therefore, $TiSi_2$ with a small ΔG_H is an active catalyst for the Heyrovsky reaction as well. To verify whether $TiSi_2$ is also good for the Tafel reaction, we further consider the dynamic process of two H atoms desorbing from the surface of $TiSi_2$. The Gibbs free energy ΔG_H of the second H atom is still close to 0 eV, and the desorbing process only needs to overcome a low energy barrier of 1.28 eV (see Figure 3c), making the Tafel reaction possible. Therefore, we can conclude that $TiSi_2$ may be a good alternative to precious Pt for the HER as it owns nearly zero free energies of hydrogen adsorption under different coverages, a low desorption energy barrier, and high electron mobility.

MgB_2 is a conventional superconductor with a high T_c of ∼40 K.[43] Its superconductivity is mainly due to boron, which strongly binds in covalent bonding.[44] The metallic nature and existing strong covalent bonding between Si atoms in $TiSi_4$ inspire us to explore its electron–phonon coupling (EPC) and potential superconductivity. The EPC calculations were performed based on Bardeen–Cooper–Schrieffer (BCS) theory[45] and derived Migdal–Eliashberg theory.[46,47] Eliashberg spectral functions (details can be found in the Supporting Information) for $TiSi_4$ are plotted in Figure 4a. All vibrational modes above 50 cm^{-1} contribute to the EPC indicated by the similarity between $F(\omega)$ and $\alpha^2F(\omega)$. The calculated EPC strength λ is 0.59, which is comparable to that of bulk CaC_6,[48] indicating reasonably strong EPC in $TiSi_4$.

The superconducting T_c is estimated using the Allen–Dynes modified McMillan equation[49,50]

$$T_c = \frac{\omega_{log}}{1.2} \exp\left[-\frac{1.04(1+\lambda)}{\lambda - \mu^*(1+0.62\lambda)}\right]$$

where μ^* is the Coulomb pseudopotential and ω_{log} is the logarithmically averaged frequency. A typical value of μ^* = 0.1 is used in the McMillan equation because there is no exact method to determine this parameter yet (the effect of μ^* on T_c is given in Figure S7). The calculated T_c is 5.8 K, exceeding the boiling point of liquid helium (4.2 K) and comparable to T_c of graphite intercalated compounds,[51,52] suggesting that $TiSi_4$ is an intrinsic BCS-type superconductor.

It is widely reported that external strain may greatly enhance the superconductivity.[53−55] Before probing the strain influence

DOI: 10.1021/acs.jpclett.6b01731
J. Phys. Chem. Lett. 2016, 7, 3723−3729

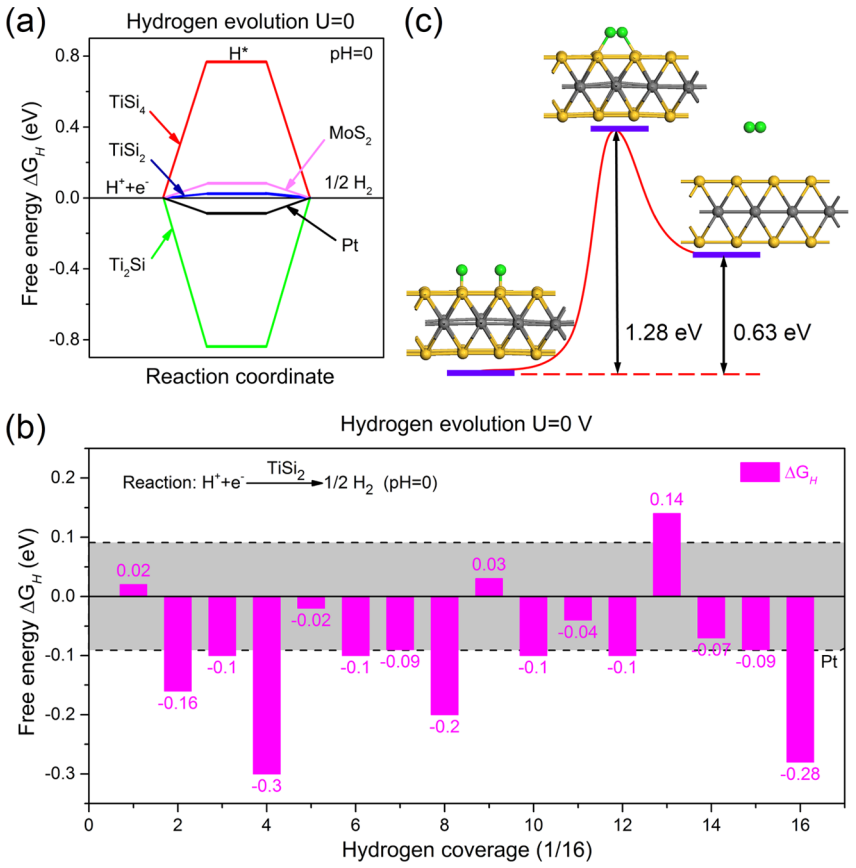

Figure 3. (a) Gibbs free energies of hydrogen adsorption ΔG_H for Ti_2Si, $TiSi_2$, and $TiSi_4$. A comparison with that of MoS_2 and Pt surface is drawn. (b) ΔG_H for different coverages in a 4 × 4 supercell of $TiSi_2$. The dashed lines denote the ΔG_H of the Pt surface (−0.09 eV) and its absolute value. (c) Calculated energy profiles involved in the recombination of two hydrogen atoms. The initial, transitional, and final structures along the paths are also given.

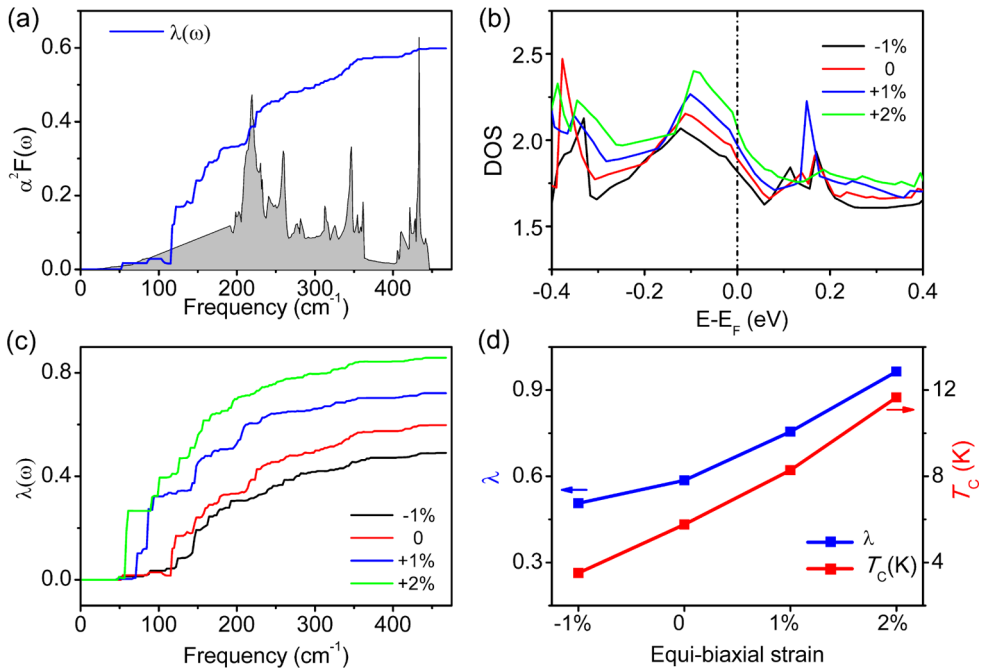

Figure 4. Superconductivity of $TiSi_4$. (a) Eliashberg spectral functions for $TiSi_4$. (b) Electronic DOS around the Fermi level for $TiSi_4$ under strain. (c) EPC $\lambda(\omega)$ for strained $TiSi_4$. (d) EPC strength λ and T_c of $TiSi_4$ as functions of equi-biaxial strains. The percentages in (b,c) denote equi-biaxial strains applied to $TiSi_4$.

DOI: 10.1021/acs.jpclett.6b01731
J. Phys. Chem. Lett. 2016, 7, 3723−3729

on the superconductivity of $TiSi_4$, it is required to find out when the dynamical instability will occur prior to the mechanical failure, as has been well studied in graphene systems.[56,57] To verify this, compressive equi-biaxial strain of $\varepsilon_{xx} = \varepsilon_{yy} = -1\%$ is first applied, and $TiSi_4$ remains dynamically stable. However, a further increase in compressive strain ($\varepsilon_{xx} = \varepsilon_{yy} = -2\%$) causes imaginary frequencies near the Γ point of the Brillouin zone, as shown in Figure S8. Tensile biaxial strains are also considered following the same thought. $TiSi_4$ can bear a tensile strain up to $\varepsilon_{xx} = \varepsilon_{yy} = +2\%$ (see Figure S8), which can be readily realized by employing suitable substrates. Figure 4b shows that the electronic DOS at the Fermi level is elevated with the increase of the tensile biaxial strain, implying the possible enhancement of EPC. We further calculate $\lambda(\omega)$ for strained $TiSi_4$ and find that both λ and T_c indeed increase with the tensile strain, as displayed in Figure 4c. The λ and T_c can be enhanced to be 0.96 and 11.7 K under a strain of +2% (see Figure 4d), which is very impressive for 2D superconductors.

In summary, we have predicted a new class of 2D materials, Ti_2Si, $TiSi_2$, and $TiSi_4$, based on a PSO global structure search and DFT calculations. They are energetically, dynamically, and thermally stable and show excellent mechanical properties. Particularly, Ti_2Si is found to be a robust ferromagnetic metal with a magnetic moment of 1.37 μ_B/cell. $TiSi_2$ is a highly active catalyst for HER with nearly zero free energies of hydrogen adsorption independent of the adsorption coverage, the low desorption energy barrier, and its high electron mobility. Most interestingly, $TiSi_4$ is a 2D phonon-mediated superconductor with comparable in-plane stiffness to graphene. Its transition temperature can be enhanced up to 11.7 K by applying a suitable strain. The versatility endows titanium silicide monolayers promising prospects for spintronic, catalytic, and superconducting applications.

COMPUTATIONAL METHODS

The PSO algorithm implemented in CALYPSO code[58,59] was employed to search 2D titanium silicide structures. In our PSO simulations, a variety of Ti_xSi_y (x = 1−4 and y = 1−4) compounds were taken into consideration. The population size and number of generation were set to be 20 and 30, respectively. For a given Ti_xSi_y, 14 atoms were considered at most in the simulation cell. For each simulation, hundreds of structures were generated, and the 6−10 energetically most favorable structures were further optimized by DFT calculations. Then, about 20 structures with energy preference and structural reasonability were further assessed by phonon dispersion calculations (see Figure S1 in the Supporting Information). Among them, only Ti_2Si, $TiSi_2$, and $TiSi_4$ are dynamically stable, and their thermal stabilities were further verified by AIMD simulations. Structure relaxations were performed with projector-augmented wave (PAW)[60] potentials and Perdew−Burke−Ernzerhof generalized gradient approximation (PBE-GGA)[61] as implemented in the Vienna ab initio simulation package (VASP).[62] We considered $3p^6 3d^2 4s^2$ and $3s^2 3p^2$ configurations as valence electrons for Ti and Si, respectively. Phonon dispersions were calculated based on density functional perturbation theory (DFPT)[63] as embedded in the Phonopy program.[64] AIMD simulations were performed using the Nosé−Hoover method[65] to control temperatures. Additionally, the climbing-image nudged elastic band (CI-NEB) method was applied to locate the minimum-energy paths and the transition states.[66] The QUANTUM ESPRESSO package[67] was used to carry out EPC calculations. More computational details are given in the Supporting Information.

ASSOCIATED CONTENT

Supporting Information

The Supporting Information is available free of charge on the ACS Publications website at DOI: 10.1021/acs.jpclett.6b01731.

Methods in detail, atomic structures and phonon dispersions of monolayers searched by CALYPSO, vibrational modes and corresponding analyses, AIMD snapshots, stress−strain relations, configurations for hydrogen adsorptions, T_c as a function of μ^*, and phonon dispersions for strained $TiSi_4$ (PDF)

AUTHOR INFORMATION

Corresponding Author

*E-mail: jlwang@seu.edu.cn.

Notes

The authors declare no competing financial interest.

ACKNOWLEDGMENTS

This work is sponsored by the NSFC (21525311, 21373045, 11404056) and NSF of Jiangsu (BK20130016) and SRFDP (20130092110029, 20130092120042) in China and the Fundamental Research Funds for the Central Universities of China. The authors acknowledge computational resources at SEU and the National Supercomputing Center in Tianjin.

REFERENCES

(1) Novoselov, K. S.; Geim, A. K.; Morozov, S. V.; Jiang, D.; Zhang, Y.; Dubonos, S. V.; Grigorieva, I. V.; Firsov, A. A. Electric Field Effect in Atomically Thin Carbon Films. *Science* **2004**, *306*, 666−669.

(2) Miró, P.; Audiffred, M.; Heine, T. An Atlas of Two-Dimensional Materials. *Chem. Soc. Rev.* **2014**, *43*, 6537−6554.

(3) Wang, Q. H.; Kalantar-Zadeh, K.; Kis, A.; Coleman, J. N.; Strano, M. S. Electronics and Optoelectronics of Two-Dimensional Transition Metal Dichalcogenides. *Nat. Nanotechnol.* **2012**, *7*, 699−712.

(4) Li, L.; Yu, Y.; Ye, G. J.; Ge, Q.; Ou, X.; Wu, H.; Feng, D.; Chen, X. H.; Zhang, Y. Black Phosphorus Field-Effect Transistors. *Nat. Nanotechnol.* **2014**, *9*, 372−377.

(5) Cao, X.; Tan, C.; Zhang, X.; Zhao, W.; Zhang, H. Solution-Processed Two-Dimensional Metal Dichalcogenide-Based Nanomaterials for Energy Storage and Conversion. *Adv. Mater.* **2016**, *28*, 6167−6196.

(6) Zhang, S.; Yan, Z.; Li, Y.; Chen, Z.; Zeng, H. Atomically Thin Arsenene and Antimonene: Semimetal-Semiconductor and Indirect-Direct Band-Gap Transitions. *Angew. Chem.* **2015**, *127*, 3155−3158.

(7) Zhang, S.; Zhou, J.; Wang, Q.; Chen, X.; Kawazoe, Y.; Jena, P. Penta-graphene: A New Carbon Allotrope. *Proc. Natl. Acad. Sci. U. S. A.* **2015**, *112*, 2372−2377.

(8) Guan, J.; Liu, D.; Zhu, Z.; Tománek, D. Two-Dimensional Phosphorus Carbide: Competition Between sp^2 and sp^3 Bonding. *Nano Lett.* **2016**, *16*, 3247−3252.

(9) Wang, Y.; Li, F.; Li, Y.; Chen, Z. Semi-Metallic Be_5C_2 Monolayer Global Minimum with Quasi-Planar Pentacoordinate Carbons and Negative Poisson's Ratio. *Nat. Commun.* **2016**, *7*, 11488.

(10) Zhang, H.; Li, Y.; Hou, J.; Tu, K.; Chen, Z. FeB_6 Monolayers: The Graphene-like Material with Hypercoordinate Transition Metal. *J. Am. Chem. Soc.* **2016**, *138*, 5644−5651.

(11) Zhuo, Z.; Wu, X.; Yang, J. Two-Dimensional Phosphorus Porous Polymorphs with Tunable Band Gaps. *J. Am. Chem. Soc.* **2016**, *138*, 7091−7098.

(12) Zhao, J.; Liu, H.; Yu, Z.; Quhe, R.; Zhou, S.; Wang, Y.; Liu, C. C.; Zhong, H.; Han, N.; Lu, J.; et al. Rise of Silicene: A Competitive 2D Material. *Prog. Mater. Sci.* **2016**, *83*, 24−151.

DOI: 10.1021/acs.jpclett.6b01731
J. Phys. Chem. Lett. 2016, 7, 3723−3729

(13) Dávila, M. E.; Xian, L.; Cahangirov, S.; Rubio, A.; Le Lay, G. Germanene: A Novel Two-Dimensional Germanium Allotrope Akin to Graphene and Silicene. *New J. Phys.* **2014**, *16*, 095002.
(14) Zhang, L.; Bampoulis, P.; Rudenko, A. N.; Yao, Q.; van Houselt, A.; Poelsema, B.; Katsnelson, M. I.; Zandvliet, H. J. W. Structural and Electronic Properties of Germanene on MoS_2. *Phys. Rev. Lett.* **2016**, *116*, 256804.
(15) Mannix, A. J.; Zhou, X.; Kiraly, B.; Wood, J. D.; Alducin, D.; Myers, B. D.; Liu, X.; Fisher, B. L.; Santiago, U.; Guest, J. R.; et al. Synthesis of Borophenes: Anisotropic, Two-Dimensional Boron Polymorphs. *Science* **2015**, *350*, 1513−1516.
(16) Feng, B.; Zhang, J.; Zhong, Q.; Li, W.; Li, S.; Li, H.; Cheng, P.; Meng, S.; Chen, L.; Wu, K. Experimental Realization of Two-Dimensional Boron Sheets. *Nat. Chem.* **2016**, *8*, 563−568.
(17) Cahangirov, S.; Topsakal, M.; Aktürk, E.; Sahin, H.; Ciraci, S. Two- and One-Dimensional Honeycomb Structures of Silicon and Germanium. *Phys. Rev. Lett.* **2009**, *102*, 236804.
(18) Penev, E. S.; Bhowmick, S.; Sadrzadeh, A.; Yakobson, B. I. Polymorphism of Two-Dimensional Boron. *Nano Lett.* **2012**, *12*, 2441−2445.
(19) Wu, X.; Dai, J.; Zhao, Y.; Zhuo, Z.; Yang, J.; Zeng, X. C. Two-Dimensional Boron Monolayer Sheets. *ACS Nano* **2012**, *6*, 7443−7453.
(20) Zhou, X.-F.; Dong, X.; Oganov, A. R.; Zhu, Q.; Tian, Y.; Wang, H.-T. Semimetallic Two-Dimensional Boron Allotrope with Massless Dirac Fermions. *Phys. Rev. Lett.* **2014**, *112*, 085502.
(21) Zhang, Z.; Yang, Y.; Gao, G.; Yakobson, B. I. Two-Dimensional Boron Monolayers Mediated by Metal Substrates. *Angew. Chem., Int. Ed.* **2015**, *54*, 13022−13026.
(22) Ma, F.; Jiao, Y.; Gao, G.; Gu, Y.; Bilic, A.; Chen, Z.; Du, A. Graphene-like Two-Dimensional Ionic Boron with Double Dirac Cones at Ambient Condition. *Nano Lett.* **2016**, *16*, 3022−3028.
(23) Lutgens, F. K.; Tarbuck, E. J. *Essentials of Geology*; Pearson Prentice Hall: Upper Sadder River, New Jersey, 2012.
(24) Luo, W.; Ma, Y.; Gong, X.; Xiang, H. Prediction of Silicon-Based Layered Structures for Optoelectronic Applications. *J. Am. Chem. Soc.* **2014**, *136*, 15992−15997.
(25) Vogt, P.; De Padova, P.; Quaresima, C.; Avila, J.; Frantzeskakis, E.; Asensio, M. C.; Resta, A.; Ealet, B.; Le Lay, G. Silicene: Compelling Experimental Evidence for Graphene-like Two-Dimensional Silicon. *Phys. Rev. Lett.* **2012**, *108*, 155501.
(26) Dai, J.; Zhao, Y.; Wu, X.; Yang, J.; Zeng, X. C. Exploration of Structures of Two-Dimensional Boron-Silicon Compounds with sp^2 Silicon. *J. Phys. Chem. Lett.* **2013**, *4*, 561−567.
(27) Ding, Y.; Wang, Y. Density Functional Theory Study of the Silicene-like SiX and XSi_3 (X = B, C, N, Al, P) Honeycomb Lattices: The Various Buckled Structures and Versatile Electronic Properties. *J. Phys. Chem. C* **2013**, *117*, 18266−18278.
(28) Ozcelik, V. O.; Cahangirov, S.; Ciraci, S. Stable Single-Layer Honeycomblike Structure of Silica. *Phys. Rev. Lett.* **2014**, *112*, 246803.
(29) Tan, X.; Li, F.; Chen, Z. Metallic BSi_3 Silicene and Its One-Dimensional Derivatives: Unusual Nanomaterials with Planar Aromatic D_{6h} Six-Membered Silicon Rings. *J. Phys. Chem. C* **2014**, *118*, 25825−25835.
(30) Huang, B.; Zhuang, H. L.; Yoon, M.; Sumpter, B. G.; Wei, S. Highly Stable Two-Dimensional Silicon Phosphides: Different Stoichiometries and Exotic Electronic Properties. *Phys. Rev. B: Condens. Matter Mater. Phys.* **2015**, *91*, 121401.
(31) Shi, Z.; Zhang, Z.; Kutana, A.; Yakobson, B. I. Predicting Two-Dimensional Silicon Carbide Monolayers. *ACS Nano* **2015**, *9*, 9802−9809.
(32) Zhu, Z.; Guan, J.; Liu, D.; Tománek, D. Designing Isoelectronic Counterparts to Layered Group V Semiconductors. *ACS Nano* **2015**, *9*, 8284−8290.
(33) Yang, J. H.; Zhang, Y.; Yin, W. J.; Gong, X. G.; Yakobson, B. I.; Wei, S. H. Two-Dimensional SiS Layers with Promising Electronic and Optoelectronic Properties: Theoretical Prediction. *Nano Lett.* **2016**, *16*, 1110−1117.
(34) Yang, L. M.; Bačić, V.; Popov, I. A.; Boldyrev, A. I.; Heine, T.; Frauenheim, T.; Ganz, E. Two-Dimensional Cu_2Si Monolayer with Planar Hexacoordinate Copper and Silicon Bonding. *J. Am. Chem. Soc.* **2015**, *137*, 2757−2762.
(35) Bader, R. F. W. *Atoms in Molecules: A Quantum Theory*; Clarendon Press: Oxford, U.K., 1994.
(36) Dumitrică, T.; Hua, M.; Yakobson, B. I. Endohedral Silicon Nanotubes as Thinnest Silicide Wires. *Phys. Rev. B: Condens. Matter Mater. Phys.* **2004**, *70*, 241303.
(37) Andrew, R. C.; Mapasha, R. E.; Ukpong, A. M.; Chetty, N. Mechanical Properties of Graphene and Boronitrene. *Phys. Rev. B: Condens. Matter Mater. Phys.* **2012**, *85*, 125428.
(38) Wang, Z.-Y.; Zhou, Y.-L.; Wang, X.-Q.; Wang, F.; Sun, Q.; Guo, Z.-X.; Jia, Y. Effects of In-Plane Stiffness and Charge Transfer on Thermal Expansion of Monolayer Transition Metal Dichalcogenide. *Chin. Phys. B* **2015**, *24*, 026501.
(39) Lukowski, M. A.; Daniel, A. S.; Meng, F.; Forticaux, A.; Li, L.; Jin, S. Enhanced Hydrogen Evolution Catalysis from Chemically Exfoliated Metallic MoS_2 Nanosheets. *J. Am. Chem. Soc.* **2013**, *135*, 10274−10277.
(40) Nørskov, J. K.; Bligaard, T.; Logadottir, A.; Kitchin, J. R.; Chen, J. G.; Pandelov, S.; Stimming, U. Trends in the Exchange Current for Hydrogen Evolution. *J. Electrochem. Soc.* **2005**, *152*, J23−J26.
(41) Pan, H. Metal Dichalcogenides Monolayers: Novel Catalysts for Electrochemical Hydrogen Production. *Sci. Rep.* **2014**, *4*, 5348.
(42) Tsai, C.; Chan, K.; Nørskov, J. K.; Abild-Pedersen, F. Rational Design of MoS_2 Catalysts: Tuning the Structure and Activity via Transition Metal Doping. *Catal. Sci. Technol.* **2015**, *5*, 246−253.
(43) Bud'ko, S. L.; Lapertot, G.; Petrovic, C.; Cunningham, C. E.; Anderson, N.; Canfield, P. C. Boron Isotope Effect in Superconducting MgB_2. *Phys. Rev. Lett.* **2001**, *86*, 1877−1880.
(44) Kortus, J.; Mazin, I. I.; Belashchenko, K. D.; Antropov, V. P.; Boyer, L. L. Superconductivity of Metallic Boron in MgB_2. *Phys. Rev. Lett.* **2001**, *86*, 4656−4659.
(45) Bardeen, J.; Cooper, L. N.; Schrieffer, J. R. Theory of Superconductivity. *Phys. Rev.* **1957**, *108*, 1175−1204.
(46) Migdal, A. B. Interactions Between Electrons and Lattice Vibrations in a Normal Metal. *Sov. Phys. JETP* **1958**, *34*, 996−1001.
(47) Eliashberg, G. M. Interactions Between Electrons and Lattice Vibrations in a Superconductor. *Sov. Phys. JETP.* **1960**, *11*, 696−702.
(48) Profeta, G.; Calandra, M.; Mauri, F. Phonon-Mediated Superconductivity in Graphene by Lithium Deposition. *Nat. Phys.* **2012**, *8*, 131−134.
(49) McMillan, W. L. Transition Temperature of Strong-Coupled Superconductors. *Phys. Rev.* **1968**, *167*, 331−344.
(50) Allen, P. B.; Dynes, R. C. Transition Temperature of Strong-Coupled Superconductors Reanalyzed. *Phys. Rev. B* **1975**, *12*, 905−922.
(51) Emery, N.; Hérold, C.; d'Astuto, M.; Garcia, V.; Bellin, C.; Marêché, J. F.; Lagrange, P.; Loupias, G. Superconductivity of Bulk CaC_6. *Phys. Rev. Lett.* **2005**, *95*, 087003.
(52) Weller, T. E.; Ellerby, M.; Saxena, S. S.; Smith, R. P.; Skipper, N. T. Superconductivity in the Intercalated Graphite Compounds C_6Yb and C_6Ca. *Nat. Phys.* **2005**, *1*, 39−41.
(53) Peng, R.; Shen, X. P.; Xie, X.; Xu, H. C.; Tan, S. Y.; Xia, M.; Zhang, T.; Cao, H. Y.; Gong, X. G.; Hu, J. P.; et al. Measurement of An Enhanced Superconducting Phase and a Pronounced Anisotropy of the Energy Gap of a Strained FeSe Single Layer in FeSe/Nb:$SrTiO_3$/$KTaO_3$ Heterostructures Using Photoemission Spectroscopy. *Phys. Rev. Lett.* **2014**, *112*, 107001.
(54) Huang, Z. C.; Pu, Y. J.; Xu, H. C.; Xu, D. F.; Song, Q.; Lou, X.; Wen, C. H. P.; Peng, R.; Feng, D. L. Electronic Structure and Superconductivity of Single-Layer FeSe on Nb:$SrTiO_3$/$LaAlO_3$ with Varied Tensile Strain. *2D Mater.* **2016**, *3*, 014005.
(55) Zhang, J.-J.; Gao, B.; Dong, S. Strain-Enhanced Superconductivity of MoX_2(X = S or Se) Bilayers with Na Intercalation. *Phys. Rev. B: Condens. Matter Mater. Phys.* **2016**, *93*, 155430.
(56) Marianetti, C. A.; Yevick, H. G. Failure Mechanisms of Graphene under Tension. *Phys. Rev. Lett.* **2010**, *105*, 245502.

DOI: 10.1021/acs.jpclett.6b01731
J. Phys. Chem. Lett. 2016, 7, 3723−3729

(57) Si, C.; Duan, W.; Liu, Z.; Liu, F. Electronic Strengthening of Graphene by Charge Doping. *Phys. Rev. Lett.* **2012**, *109*, 226802.
(58) Wang, Y.; Lv, J.; Zhu, L.; Ma, Y. Crystal Structure Prediction via Particle-Swarm Optimization. *Phys. Rev. B: Condens. Matter Mater. Phys.* **2010**, *82*, 094116.
(59) Wang, Y.; Miao, M.; Lv, J.; Zhu, L.; Yin, K.; Liu, H.; Ma, Y. An Effective Structure Prediction Method for Layered Materials Based on 2D Particle Swarm Optimization Algorithm. *J. Chem. Phys.* **2012**, *137*, 224108.
(60) Blöchl, P. E. Projector Augmented-wave Method. *Phys. Rev. B: Condens. Matter Mater. Phys.* **1994**, *50*, 17953−17979.
(61) Perdew, J. P.; Burke, K.; Ernzerhof, M. Generalized Gradient Approximation Made Simple. *Phys. Rev. Lett.* **1996**, *77*, 3865−3868.
(62) Kresse, G.; Furthmüller, J. Efficient Iterative Schemes for *ab initio* Total-Energy Calculations Using a Plane-wave Basis Set. *Phys. Rev. B: Condens. Matter Mater. Phys.* **1996**, *54*, 11169−11186.
(63) Baroni, S.; De Gironcoli, S.; Dal Corso, A.; Giannozzi, P. Phonons and Related Crystal Properties from Density-Functional Perturbation Theory. *Rev. Mod. Phys.* **2001**, *73*, 515−562.
(64) Togo, A.; Oba, F.; Tanaka, I. First-Principles Calculations of the Ferroelastic Transition Between Rutile-type and $CaCl_2$-type SiO_2 at High Pressures. *Phys. Rev. B: Condens. Matter Mater. Phys.* **2008**, *78*, 134106.
(65) Martyna, G. J.; Klein, M. L.; Tuckerman, M. Nosé-Hoover Chains: The Canonical Ensemble via Continuous Dynamics. *J. Chem. Phys.* **1992**, *97*, 2635−2643.
(66) Henkelman, G.; Uberuaga, B. P.; Jónsson, H. A Climbing Image Nudged Elastic Band Method for Finding Saddle Points and Minimum Energy Paths. *J. Chem. Phys.* **2000**, *113*, 9901−9904.
(67) Giannozzi, P.; Baroni, S.; Bonini, N.; Calandra, M.; Car, R.; Cavazzoni, C.; Ceresoli, D.; Chiarotti, G. L.; Cococcioni, M.; Dabo, I.; et al. QUANTUM ESPRESSO: A Modular and Open-Source Software Project for Quantum Simulations of Materials. *J. Phys.: Condens. Matter* **2009**, *21*, 395502.

DOI: 10.1021/acs.jpclett.6b01731
J. Phys. Chem. Lett. 2016, 7, 3723−3729